energies

MDPI

Article

Using the Method of Harmonic Distortion Analysis in Partial Discharge Assessment in Mineral Oil in a Non-Uniform Electric Field

Alper Aydogan [1], Fatih Atalar [1], Aysel Ersoy Yilmaz [1] and Pawel Rozga [2,*]

[1] Department of Electrical and Electronic Engineering, Istanbul University-Cerrahpaşa, 34320 Avcilar, Istanbul, Turkey; aydoganalper@gmail.com (A.A.); fatih.atalar@istanbul.edu.tr (F.A.); aersoy@istanbul.edu.tr (A.E.Y.)

[2] Institute of Electrical Power Engineering, Lodz University of Technology, 90-924 Łódź, Poland

* Correspondence: pawel.rozga@p.lodz.pl; Tel.: +48-609-725-622

Received: 21 August 2020; Accepted: 14 September 2020; Published: 15 September 2020

Abstract: In high-voltage equipment, it is vital to detect any failure in advance. To do this, a determination of the partial discharges occurring at different voltage types as well as at different electrode configurations is essential for observing the oil condition. In this study, an experimental setup consisting of a needle–semi-sphere electrode configuration immersed in mineral oil is prepared for laboratory experiment. In such a way, a non-uniform electric field is created and the leakage currents are monitored from the grounded electrode. A total of six different electrode configurations are analyzed during the tests by the use of hemispheres of different diameters as grounded electrodes and copper and steel pointed (medical) needle high-voltage electrodes. In the experiments, the partial discharges occurring at four different voltage levels between 5.4 and 10.8 kV are measured and recorded. The effect of the different electrode configurations and voltage levels on the harmonic distortion are noted and discussed. It is experimentally confirmed that it is possible to measure the leakage current caused by the partial discharges of the corona type in oil at the different metal points, creating high-voltage electrodes and different electric field distributions based on the proposed non-invasive measurement technique. The studies showed that there is a significant rise of even harmonic components in the leakage current during the increase in the partial discharge intensity with the 5th harmonic as dominant.

Keywords: partial discharge; mineral oil; harmonic distortion; non-uniform electric field; discrete Fourier transform

1. Introduction

The insulation quality of power transformers, cables, or circuit breakers, being the main devices used in high-voltage transmission systems, is very important from the point of view of ensuring sustainable and reliable electrical energy for end users [1]. Dielectric liquids, which have been applied in the mentioned devices as a sole insulation or as a part of a combined insulation system, have been extensively used since the 1850s. The main dielectric liquid applied in high-voltage equipment has been mineral oil, however other liquids such as silicone oils, synthetic esters, and natural esters have been used as well [2]. Although dielectric liquids are easy to implement in the insulating systems and provide electrical insulation effectively, they are very sensitive to impurities due to their specific chemical structure. In particular, pollutant materials within the structure such as solid particles [3,4], gas bubbles [5], or water droplets [6,7] greatly reduce the dielectric performance of insulating liquids [8]. There are many methods, such as, for example, the AC breakdown voltage and dielectric dissipation factor measurement, gas chromatography, and the determination of the moisture content in oil, which are used to estimate the condition of a given dielectric liquid [9,10]. In turn, the experiments

focused on the obtainment of the electrical strength and dielectric characteristics of liquids, which are the determinants of their use as proper insulators in high-voltage insulating systems [11,12].

When the dielectric liquid is used as insulation partial discharges (PDs), this constitutes a significant problem for the functioning of the insulating system. Partial discharges refer to the events that occur in the insulating system, deteriorating partially the existing insulation [13], and are also defined as partial breakdowns in the cavities in the insulation due to the high electric field [14]. When assessing partial discharges, including the detection, measurement, and location of PD sources, various effects and physical phenomena accompanying partial discharges are identified, such as the presence of current pulses and the associated emission of electromagnetic waves, chemical changes in insulating materials, the emission of acoustic waves, the emission of light radiation, local temperature increases in the discharge channel or increasing the pressure in the discharge channel [15–17]. The fast aperiodic current pulses with a rise time of the order of nanoseconds that accompany the partial discharges are the source of radiated and conducted disturbances. When the electromagnetic waves are considered, they may cover the range of light radiation. The light emission results from de-excitation processes and ion recombination. Depending on the medium in which the discharge takes place (air, SF_6, oil) and atmospheric factors (temperature, pressure), the emission spectrum is in the range of UV and infrared wavelengths. Part of the energy released during partial discharges changes into mechanical energy in the form of the above-mentioned acoustic signals propagating in all directions, subject to the phenomena of attenuation, reflection, refraction, and dispersion. The amplitude of the acoustic emission pulses is inversely proportional to the distance from the discharge source, and the intensity of the acoustic emission is inversely proportional to the square of the distance. A single partial discharge, which can be compared to a micro-explosion, affects the area covered by the phenomenon, causing a change in the physical properties of the dielectric. As the physical properties of insulating material change, they reflect in changes in the dielectric dissipation factor (tg δ). The system in which PDs do not occur is characterized by a relatively constant value of tg δ, while when the PDs appear their intensity causes an increase in the tg δ. The chemical transformations resulting from partial discharges largely depend on the design of the device and the dielectric materials used in it. The most important chemical transformations resulting from partial discharges are gas evolution, the surface erosion of materials, or electric wood formation. Considering mineral oil-based insulation, the processes connected with PDs give reflection in the generation of specific types of gases as a result of the chemical degradation of oil or oil-paper combined insulation due to electrical or thermal stresses. In a more macroscopic scale, the partial discharges have also a significant influence on the energy and power losses resulting from ionization processes associated with PDs or disturbances in the supplying voltage and current (the possible occurrence of harmonic distortion) [15–33].

There are few direct or indirect methods which are commonly used to detect partial discharges in insulating systems with liquid dielectrics and to assess their intensity. The widely known indirect method is gas chromatography (called dissolved gas analysis—DGA), in which the gases generated due to partial discharges (or other electrical and thermal events) may be collected and analyzed. This method is also referred to as a chemical method. The oil condition is assessed from the measured gas concentrations on the basis of comparison with typical values given in standards or on the basis of a developed analysis method, such as, for example, the Duval triangle method [9,18]. During oil analysis from gas chromatography, it is important to point out that also other oil parameters must be evaluated, such as the moisture content, dielectric dissipation factor, AC breakdown voltage, etc. Another non-electrical PD measurement method is the acoustic emission (AE) method [19,20]. It is a non-invasive method allowing for the determination of the place of partial discharge occurrence and also its type (corona discharge, surface discharge, internal discharge in cavities) by registering the acoustic wave generated by the discharge. PDs may be analyzed also using Ultra High Frequency (UHF) detection. This method has been extensively studied in recent years, mainly as a promising method for use in the condition monitoring of power transformers. However, many tests of the UHF method have been performed on experimental systems with mineral oil as the dielectric liquid [21,22].

In this method, the partial discharge data of different frequency components are evaluated in the range of ultra-high frequency radiation, and the identification of PD types may be performed on the basis of the information obtained in this way. Some works report also the use of light emitted by partial discharges for the assessment of discharge intensity. A qualitative assessment may be conducted on the basis discharge images, as in [23], or the spectra of emitted light may be compared to conclude on the discharge behavior [24].

In addition to the above-mentioned indirect, non-invasive methods of PD analysis of the oil-insulated systems, the most reliable method is still the electrical method based on IEC 60270 Standard [7]. By means of a specially designed testing system, a quantitative assessment of PD intensity is possible. The apparent charge, measured typically in picocoulombs (pC), and the phase-resolved partial discharge (PRPD) patterns recorded during measurement may give the valuable data on the insulating system condition determined by the insulating components' quality [9,16,25]. Typically, the process of data collection is determined by increasing the testing voltage gradually and the registration of the PD signals during the whole process or in time intervals. Partial discharge inception voltage (PDIV) is determined, and PD behavior at higher values of voltage than PDIV is observed. In experimental laboratory studies, a comparison of the different factors influencing the PD intensity (electrode configurations, liquid kind) may be carried out in this way.

There are many works which have been devoted to the problem of PD detection and analysis, with many different points of view on this issue presented by the authors [16,26–32]. Chen et al. experimentally modeled PD behavior in oil-impregnated paper-insulated transformers. Sudden increases in PDs were the determinant in the evaluation of partial discharge-based failures. The authors of the mentioned paper found that average value of PDs is more determinant in asymmetric electrode systems [26]. Gulski et al., in a fundamental work [27], analyzed the deterioration behavior of different insulating materials in high-voltage electrical systems. In the study, the surface discharges and corona discharges in transformer oil were investigated as well. They created and monitored PDs and analyzed the PRPD patterns obtained from the data collected. They found that it is possible to determine the type of partial discharge failure as a result of this form of analysis [27,28]. Cavallini et al. examined the characteristic patterns of PDs in a current transformer and resin. They showed that it is possible to detect other sources of noise on the basis of their studies [29,30]. In addition, Contin et al. have studied major mathematical models used to characterize partial discharge waveforms. They analyzed and evaluated the behavior of the high-frequency current transformer sensors used to collect the original partial discharge signal (symmetrical PD pulse signal and asymmetric PD pulse signal) found in mathematical models [31]. Alvarez et al. have obtained results that successfully measure common PD sources (corona, surface discharges, and internal discharges) by defining the source of signals collected from different partial discharge and noise sources in distribution systems and pulse sources that were mathematically evaluated and classified [32]. The statistical-based approach was presented, however, in [16], where different PD analysis techniques (electrical method, acoustic emission, and UHF) were compared. The authors found that every method was characterized by different properties and restrictions, so the different fields of application and specific measurement condition requirements need to be supported. Additionally, they indicated on a need for conducting further research works connected with the development of a method of PD source detection and identification in insulating systems with oil insulation.

Taking this latter into account, in the studies presented in this paper the behavior of partial discharges was investigated by means of the authors' approach based on the leakage current monitoring from the grounded electrode of the experimental system considered. Thus, the goal of the studies was to confirm the possibility of analyzing the PD intensity quantitively on the basis of the collected current signals, which will be then analyzed using discrete Fourier transform. A non-uniform electric field system was created to do that by using a needle–hemisphere electrode configuration immersed in mineral oil. Two different pointed-type high-voltage electrodes (one made of steel and the second made of copper) and three different-in-radius hemisphere electrodes (2, 5, and 6 cm) were applied to

note the possible influence of different factors on the registered courses. The current signals at the selected voltage levels were sampled at a frequency level of 6250 Hz.

2. Mathematical Formulation

Harmonic analysis is one of the most frequently used methods to find the failure of high-voltage, medium-voltage, and low-voltage electrical and electronic systems. When the transmission and distribution lines are examined, external factors such as severe atmospheric conditions and some other stresses like electric or thermal problems may cause insulation deterioration. This leads to the formation of non-sinusoidal wave shapes. Harmonic components can be used to estimate the physical and dielectric conditions. To calculate the harmonic components, generally Fourier transform is used. A Fourier transform of a function $f(t)$ is shown in well-known Equation (1):

$$F(\omega) = \int_{-\infty}^{\infty} f(t)e^{-j\omega t}dt \tag{1}$$

where $F(\omega)$ is the function in the frequency domain for $f(t)$ and ω is the angular frequency of the system.

The function may be also converted from the frequency domain to the time domain by Equation (2).

$$f(t) = \frac{1}{2\pi}\int_{-\infty}^{\infty} F(\omega)e^{-j\omega t}dt \tag{2}$$

When n samples are taken for each period, periodically sampled functions can be obtained by using Equations (1) and (2). Discrete Fourier transform is shown in Equations (3) and (4), in which normal and inverse transformation are possible, respectively.

$$F(k\Delta\Omega) = \sum f(n\Delta T)e^{-j2\pi kn/N} \tag{3}$$

$$F(n\Delta T) = \sum f(k\Delta\Omega)e^{-j2\pi kn/N} \tag{4}$$

Considering Equation (3), $k, n = 0, 1, \ldots, N-1$, where n is the sampling number in the time domain and $\boldsymbol{k}$ is the sampling number in the frequency domain, N represents the total number of samples.

$\Delta\Omega = 2\pi/\Delta T$ and $\Delta T = T/N$ are used to calculate the change in time and change in frequency, respectively. Discrete Fourier Transform (DFT) is often used in harmonic measurements, as it is taken as measurement information which can be obtained as the sampling function in the time domain. Since DFT is set off as measurement information in the form of the sampling function in the time domain, it is often used for measuring the harmonic component values.

Fast Fourier Transform (FFT) is used to facilitate discrete Fourier transform, as shown in Equation (5), by using the similarity of the elements in the matrix $[\boldsymbol{W^{kn}}]$.

$$W = e^{-2j\pi/N} \tag{5}$$

Following this result, the number of transactions decreases to the $(N{\cdot}log_2(N))$ level.

To analyze the non-sinusoidal current values, Fourier transform is used, as in Equation (6).

$$i(t) = \sum_{n=1}^{\infty} i_n(t) = \sum_{n=1}^{\infty} \sqrt{2}I_n sin(n\omega_1 t + \delta_n) \tag{6}$$

In the above equation, the DC terms are neglected. In the time domain, the nth degree is the instantaneous value of the harmonic current. It is the effective value of harmonic current at the nth degree, ω_1 is the angular frequency of the base frequency, and δ_n is the phase angle of the harmonic current at the nth degree.

The harmonic distortion (*HD*) of any current signal can be calculated in Equation (7).

$$HD_n = \frac{I_n}{I_1} \tag{7}$$

The corresponding current for the ***n*** order harmonic is expressed as the relative harmonic current.

3. Experimental Setup and Measurement Methodology

An experimental setup for leakage current measurement under a high voltage was established for the laboratory studies. A schematic representation of this setup is shown in Figure 1.

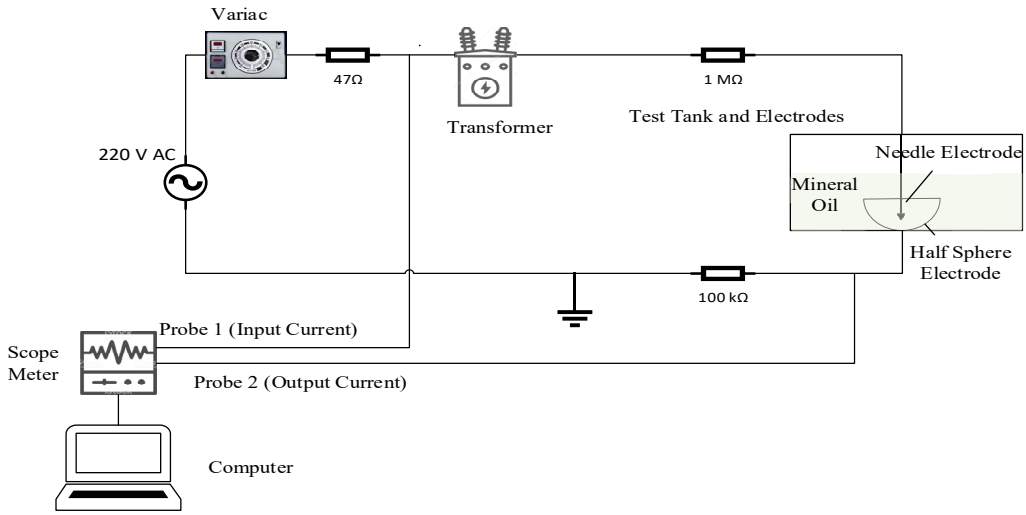

Figure 1. Experimental setup and circuit diagram.

The voltage adjusted by a Variac autotransformer (Varsan brand) with 5 kVA power and a 0–220 V range at the 50 Hz frequency level was applied to the primary winding of the voltage transformer. The voltage transformer VTB 30–200 (Esitas brand) has a conversion ratio of 220 V/40 kV, with a rated power of 1.5 kVA. No deterioration in the signal of the voltage applied was observed during the pre-studies. A 1 MΩ limiting resistance was placed on the high-voltage side of the transformer, as it is typically applied in high-voltage laboratory measurements to protect against high current during breakdown in the testing system [11,12,16,33]. The input current was measured via a 47 Ω resistor at the Variac output, while the output current was measured via a 100 kΩ resistor connected to the ground electrode. The input and output currents corresponding with PD events were measured with a Fluke meter 190–504/EU/S, which has 200 MHz bandwidth oscilloscope with a sampling rate of 2.5 GS/s (Giga Sample/second), with an accuracy of 2.1% of reading + 0.04 × range/div. The current probes used were, however, in both cases (Probe 1 and Probe 2 from Figure 1) the Fluke-branded vps410-ii-v models. Since the approach of the studies was to analyze the signals of leakage current from the grounded electrode, the signal from Probe 2 was further analyzed using FFT. The data of the measured values were taken by FlukeView® SW160 for the MultiFunction Counter interface software. It is important to point out herein that the 47 Ω resistor used does not affect the experimental results, understood as a distortion of the source signal. The primary and secondary voltage of the HV transformer were, however, measured by the Fluke 80 K–40 HV Probe and True RMS Multimeter. The actual photograph of the circuit used is presented in Figure 2.

During each test, a total number of 30,000 data points was obtained during the 4.8 s of measurement. Thus, the sampling frequency was 6250 Hz, and the leakage current data were obtained and read solely by this specific mode of the oscilloscope used. The full sampling size of the oscilloscope was not applied. None of the smoothing windows methods were used, and signals were drawn over the −/+2 Hz adjacent of the frequency for the specified harmonic values. For example, the signals

between 148 and 152 Hz for the 3rd harmonic were evaluated. Additionally, frequency leakage was not a concern.

The sensitivity of the experiments was kept stable in terms of unwanted effects. All of the data considered just belonged to leakage currents and harmonic distortions of the PDs. Additionally, there was no deterioration in the applied testing voltage that may affect the experiment. In the main feed of the laboratory, clean sine was provided through filters.

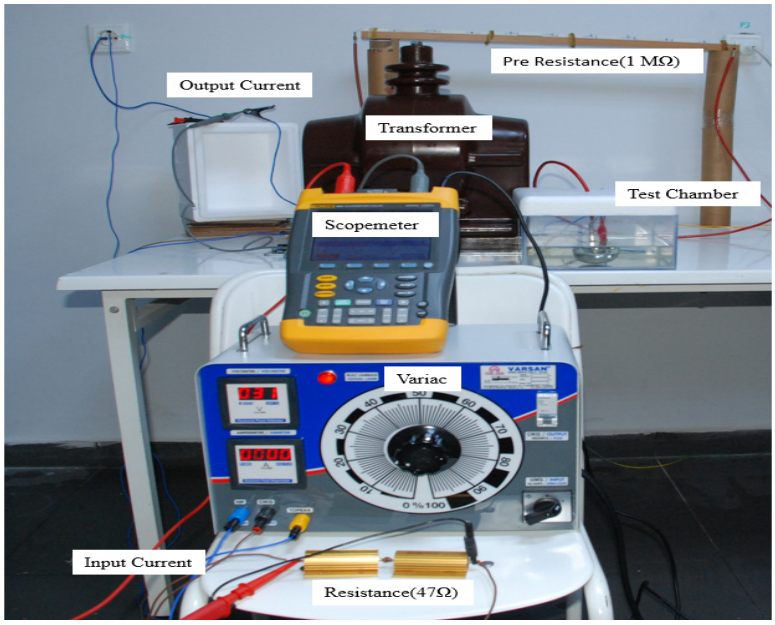

Figure 2. Photograph of the experimental setup.

A classical FFT analysis of the data collected was driven with Matlab software. It was determined how much amplitude the signal has and at which frequency.

The test chamber from Figure 2 is made of plexiglass and has dimensions of 25 × 25 × 10 cm. Mineral oil with a dielectric constant of 2.2 was used throughout the experiments as the dielectric liquid under test. The oil before the beginning of the experiment fulfilled the requirements for the mineral oil specified in the IEC 60296 Standard [34].

In this study, three different hemispheres made of pure copper with the diameters of 6, 5, and 2 cm were used as the grounded electrodes, respectively. Steel (medical) and copper-pointed needles especially prepared for the experiment, both with a tip radius of 0.1 μm, were however used as high-voltage (HV) electrodes. All the electrode configurations are listed in Table 1.

Table 1. Electrode configurations.

Electrode Configuration	Electrode 1 (Half-Sphere Diameter)	Electrode 2 (Tip Point Radius)
A	6 cm copper	0.1 μm copper
B	6 cm copper	0.1 μm steel
C	5 cm copper	0.1 μm copper
D	5 cm copper	0.1 μm steel
E	2 cm copper	0.1 μm copper
F	2 cm copper	0.1 μm steel

For each electrode configuration five electrode ranges (gap distances) were considered from 1 mm to 5 mm with increasing steps of 1 mm. The term "electrode range" is defined as the distance between the end of the needle and the deeper point of the semi-sphere consisting of a grounded electrode. The HV electrodes were changed in every different electrode gap. This was done because the tip point

of the needle electrode was worn down due to the high voltage stress. As was reported in many publications [11,16,33,35,36], the degree of damage to the needle tip is believed to be a reflection of the extremely high temperatures prevailing during the discharge processes, especially at breakdown (electrical arc). An electrical arc has a high energy because the electron avalanches increase in a cumulative way, and at the end of this phenomenon a conductive bridge occurs from the tip point of the electrode to the deep mid-point of the hemisphere-grounded electrode. Hence, the temperature of the tip point of the HV electrode gradually increases. While the PDs continue, more and more electrons give way from the tip point of the HV electrode. Excessive increment in both the temperature and numbers of moving electrons causes damage to the point of the HV electrode.

The experiments were conducted under four pre-selected voltage levels, which were 5.4, 7.2, 9, and 10.8 kV, respectively. The selected values resulted from the limitations of the used supplying system, where voltage might be set with 1.8 kV steps. At the 5.4 kV voltage level, the meaningful and comparable data started to be obtained. In turn, for the tests performed at voltages of over 10.8 kV, healthy data could not be obtained with the measuring instruments applied. Therefore, to protect the measuring instruments, the experiment was terminated at the voltage level of 10.8 kV.

The test chamber used in the experiment was specially sketched and designed. All the dimensions were predefined for the purpose of the experiment. In addition, the positions and distances between the electrodes were specially designed in a millimeter range. Hence, hemispherical and needle electrodes could adapt their position in this delicate range. During the experiment, the HV electrodes were aligned exactly to the midpoint of the hemisphere. The above approach enabled the repeatability of the measurement process.

Sample data of 20 periods were selected and analyzed according to each voltage level.

4. Results and Discussion

At first, Table 2 presents the complex results of the HD values for each electrode configuration at characteristic voltage levels obtained separately for each electrode range. However, in the further part of the paper, the distinctive configurations are analyzed separately with some relations to each other.

Table 2. HD values for each electrode configuration at characteristic voltage levels.

Electrode Configuration	Voltage (kV)	d (mm)	HD_2	HD_3	HD_4	HD_5	HD_6	HD_7	HD_8	HD_9
A	5.4	1	0.0299	0.0094	0.0196	0.0736	0.0252	0.0238	0.0199	0.0373
A	5.4	2	0.0424	0.0062	0.0571	0.0911	0.0534	0.0265	0.0427	0.0427
A	5.4	3	0.0444	0.0122	0.0476	0.108	0.0401	0.0125	0.0333	0.0538
A	5.4	4	0.0497	0.0108	0.0429	0.076	0.0527	0.0343	0.0482	0.0267
A	5.4	5	0.0359	0.0192	0.0344	0.0809	0.0267	0.0258	0.021	0.0247
A	7.2	1	0.0448	0.007	0.0446	0.0701	0.0424	0.0192	0.0332	0.0368
A	7.2	2	0.0492	0.0101	0.0458	0.0768	0.0452	0.0202	0.0345	0.0379
A	7.2	3	0.0331	0.0091	0.0364	0.0794	0.0382	0.0341	0.0325	0.0307
A	7.2	4	0.0222	0.0121	0.0394	0.0766	0.0378	0.035	0.0338	0.0325
A	7.2	5	0.0418	0.0112	0.0253	0.079	0.0296	0.0267	0.0219	0.0223
A	9	1	0.0186	0.0068	0.0135	0.0855	0.0168	0.0213	0.0174	0.0348
A	9	2	0.0261	0.0071	0.0218	0.0783	0.0241	0.03	0.018	0.0383
A	9	3	0.0304	0.0091	0.0323	0.0761	0.0377	0.0337	0.0299	0.0359
A	9	4	0.0299	0.0117	0.022	0.0831	0.0258	0.0283	0.0179	0.0343
A	9	5	0.0375	0.0086	0.0294	0.0723	0.0322	0.0265	0.0188	0.0372
A	10.8	1	0.0125	0.0066	0.0115	0.078	0.018	0.0264	0.0165	0.0313
A	10.8	2	0.0245	0.0079	0.0169	0.0864	0.0246	0.0252	0.0126	0.0464
A	10.8	3	0.0254	0.0063	0.0233	0.0691	0.0251	0.0179	0.0223	0.0337
A	10.8	4	0.025	0.009	0.0154	0.085	0.0279	0.0238	0.0273	0.0326
A	10.8	5	0.0288	0.0084	0.0271	0.078	0.032	0.0257	0.029	0.0315
B	5.4	1	0.0622	0.0138	0.0408	0.065	0.053	0.0214	0.0527	0.023
B	5.4	2	0.0842	0.0106	0.052	0.0833	0.0268	0.026	0.0464	0.0195
B	5.4	3	0.0667	0.0112	0.0457	0.089	0.0301	0.0297	0.0354	0.0293
B	5.4	4	0.1028	0.0096	0.0621	0.0668	0.0283	0.0329	0.0377	0.0256
B	5.4	5	0.0611	0.0164	0.0578	0.0965	0.039	0.0357	0.0288	0.0219

Table 2. *Cont.*

Electrode Configuration	Voltage (kV)	d (mm)	HD_2	HD_3	HD_4	HD_5	HD_6	HD_7	HD_8	HD_9
B	7.2	1	0.0352	0.0071	0.0177	0.0662	0.0246	0.0106	0.0274	0.0361
B	7.2	2	0.0524	0.0108	0.025	0.0891	0.0239	0.023	0.033	0.0214
B	7.2	3	0.0492	0.0067	0.0264	0.0659	0.0341	0.0136	0.045	0.0299
B	7.2	4	0.0425	0.0111	0.028	0.0752	0.0229	0.0159	0.0286	0.0333
B	7.2	5	0.0551	0.0091	0.0271	0.0693	0.0443	0.0278	0.0676	0.0348
B	9	1	0.0227	0.0082	0.0176	0.0826	0.0269	0.0112	0.0256	0.0343
B	9	2	0.056	0.0133	0.0336	0.0895	0.0241	0.018	0.031	0.028
B	9	3	0.0403	0.0075	0.0183	0.0696	0.0345	0.0191	0.0427	0.03
B	9	4	0.0356	0.0102	0.016	0.067	0.0237	0.0046	0.0336	0.0312
B	9	5	0.0343	0.0091	0.0209	0.083	0.0192	0.0225	0.0207	0.0296
B	10.8	1	0.0273	0.0093	0.0094	0.0622	0.0175	0.0247	0.0183	0.0284
B	10.8	2	0.0433	0.012	0.013	0.0812	0.0221	0.0135	0.0184	0.0275
B	10.8	3	0.032	0.0062	0.0101	0.0745	0.0163	0.0216	0.0222	0.0343
B	10.8	4	0.0385	0.0118	0.0204	0.0756	0.016	0.0188	0.018	0.0328
B	10.8	5	0.0304	0.0059	0.0182	0.0819	0.0184	0.0114	0.0233	0.03
C	5.4	1	0.0591	0.0137	0.0474	0.0526	0.0508	0.0453	0.0429	0.0334
C	5.4	2	0.0652	0.0134	0.0408	0.0626	0.037	0.0287	0.0302	0.0404
C	5.4	3	0.069	0.0146	0.0509	0.0842	0.0538	0.0164	0.0376	0.0532
C	5.4	4	0.0725	0.0115	0.0593	0.092	0.0756	0.0311	0.067	0.0369
C	5.4	5	0.054	0.0118	0.0403	0.0764	0.0521	0.0347	0.0466	0.0313
C	7.2	1	0.0379	0.0143	0.0239	0.0599	0.0279	0.0483	0.0161	0.0362
C	7.2	2	0.0326	0.0087	0.0207	0.0638	0.0286	0.0355	0.0222	0.0364
C	7.2	3	0.0599	0.0057	0.0476	0.0758	0.0458	0.0192	0.0371	0.0454
C	7.2	4	0.0387	0.0114	0.0291	0.0784	0.0345	0.0237	0.0299	0.0314
C	7.2	5	0.0348	0.0098	0.0252	0.081	0.039	0.0308	0.0325	0.0358
C	9	1	0.0358	0.0082	0.0291	0.0757	0.0341	0.0273	0.0321	0.0397
C	9	2	0.0301	0.005	0.02	0.0756	0.0206	0.0225	0.0149	0.0411
C	9	3	0.0443	0.0078	0.0346	0.0668	0.0343	0.0373	0.0204	0.0327
C	9	4	0.0355	0.0102	0.0327	0.0749	0.0365	0.0328	0.0296	0.0323
C	9	5	0.0295	0.0117	0.0215	0.0856	0.0344	0.0375	0.0278	0.0322
C	10.8	1	0.0149	0.0063	0.0067	0.0743	0.0135	0.0294	0.0136	0.0399
C	10.8	2	0.0285	0.0052	0.0186	0.0737	0.0178	0.0356	0.0099	0.04
C	10.8	3	0.0233	0.0061	0.0179	0.0742	0.0244	0.0286	0.0155	0.0348
C	10.8	4	0.0298	0.0105	0.0194	0.087	0.0213	0.0259	0.0162	0.0468
C	10.8	5	0.0317	0.0064	0.0259	0.0774	0.0304	0.0321	0.0208	0.0447
D	5.4	1	0.0582	0.0173	0.0418	0.0545	0.0454	0.0511	0.0395	0.0237
D	5.4	2	0.0662	0.0102	0.0654	0.0584	0.0613	0.0585	0.0456	0.0513
D	5.4	3	0.0766	0.0061	0.0676	0.0603	0.0672	0.0404	0.0677	0.0485
D	5.4	4	0.0653	0.0141	0.0513	0.0661	0.0452	0.0559	0.0325	0.056
D	5.4	5	0.054	0.0126	0.0364	0.0738	0.0396	0.0388	0.0421	0.05
D	7.2	1	0.0534	0.0082	0.0427	0.0718	0.0411	0.0371	0.0254	0.0366
D	7.2	2	0.0438	0.0085	0.0411	0.0695	0.0427	0.0454	0.0285	0.0551
D	7.2	3	0.0509	0.0117	0.0429	0.0717	0.0383	0.0422	0.0295	0.0485
D	7.2	4	0.0435	0.0127	0.0393	0.0739	0.0378	0.0333	0.0364	0.0482
D	7.2	5	0.0493	0.0068	0.0431	0.0732	0.0475	0.0358	0.039	0.0508
D	9	1	0.039	0.0063	0.0294	0.0624	0.0363	0.0423	0.0343	0.0425
D	9	2	0.0334	0.011	0.0301	0.071	0.0284	0.0382	0.0189	0.0535
D	9	3	0.0379	0.0085	0.0334	0.0664	0.0335	0.0492	0.0242	0.0606
D	9	4	0.0326	0.0056	0.0311	0.0717	0.0296	0.041	0.0316	0.0485
D	9	5	0.0461	0.0089	0.0407	0.0708	0.041	0.0513	0.0209	0.049
D	10.8	1	0.0267	0.0094	0.0203	0.0546	0.0201	0.0347	0.0109	0.0476
D	10.8	2	0.0321	0.0052	0.0311	0.0673	0.0292	0.0426	0.0213	0.051
D	10.8	3	0.0362	0.0079	0.0264	0.0608	0.0255	0.035	0.017	0.061
D	10.8	4	0.0233	0.0049	0.0179	0.0754	0.021	0.0415	0.0193	0.0544
D	10.8	5	0.0415	0.0079	0.0316	0.0725	0.03	0.0383	0.0165	0.0642
E	5.4	1	0.0106	0.0119	0.0028	0.0767	0.0045	0.0372	0.0032	0.0447
E	5.4	2	0.0198	0.0096	0.005	0.0731	0.0039	0.0392	0.0046	0.0463
E	5.4	3	0.009	0.0136	0.0021	0.0785	0.0035	0.0386	0.0038	0.0509
E	5.4	4	0.012	0.0138	0.0048	0.0818	0.0025	0.0401	0.0062	0.0438
E	5.4	5	0.0132	0.012	0.0051	0.0856	0.0043	0.035	0.0056	0.0441
E	7.2	1	0.0067	0.01	0.0059	0.0799	0.0033	0.0326	0.0031	0.0448
E	7.2	2	0.0225	0.009	0.0073	0.0839	0.0057	0.036	0.0058	0.0535
E	7.2	3	0.0097	0.0088	0.0095	0.0865	0.0042	0.0331	0.0054	0.0467
E	7.2	4	0.0095	0.0101	0.0087	0.08	0.0033	0.0382	0.0061	0.0453

Table 2. *Cont.*

Electrode Configuration	Voltage (kV)	d (mm)	HD_2	HD_3	HD_4	HD_5	HD_6	HD_7	HD_8	HD_9
E	7.2	5	0.0108	0.0089	0.0102	0.0817	0.0043	0.032	0.0066	0.0434
E	9	1	0.0241	0.0106	0.0083	0.0812	0.004	0.0339	0.0042	0.0417
E	9	2	0.0188	0.0115	0.0094	0.0737	0.0027	0.0366	0.0088	0.0398
E	9	3	0.0106	0.0083	0.0049	0.0803	0.0071	0.0386	0.0026	0.044
E	9	4	0.0101	0.0092	0.0036	0.0728	0.0066	0.0328	0.0048	0.0458
E	9	5	0.0113	0.0092	0.0055	0.0742	0.0064	0.038	0.0043	0.0426
E	10.8	1	0.0263	0.0074	0.0044	0.0787	0.0055	0.0254	0.0037	0.0489
E	10.8	2	0.0211	0.0109	0.0042	0.0804	0.0074	0.0353	0.0049	0.0413
E	10.8	3	0.0107	0.0137	0.006	0.077	0.0055	0.0371	0.0046	0.0467
E	10.8	4	0.0119	0.0123	0.0063	0.0796	0.0048	0.0373	0.0061	0.0452
E	10.8	5	0.2206	0.1052	22.253	0.0824	0.1706	0.2423	2.882	0.4432
F	5.4	1	0.0102	0.0093	0.0044	0.0604	0.0067	0.0357	0.0074	0.0675
F	5.4	2	0.0145	0.0082	0.0049	0.0728	0.0069	0.0474	0.0087	0.0609
F	5.4	3	0.0151	0.0076	0.0063	0.0704	0.0076	0.0503	0.0089	0.0611
F	5.4	4	0.0102	0.005	0.0088	0.0723	0.0063	0.0451	0.0051	0.0621
F	5.4	5	0.0109	0.0097	0.0056	0.069	0.0056	0.0484	0.0071	0.0718
F	7.2	1	0.011	0.0081	0.0074	0.0742	0.0067	0.0448	0.0095	0.058
F	7.2	2	0.0106	0.0075	0.0084	0.0717	0.0074	0.0476	0.0066	0.0611
F	7.2	3	0.0106	0.0058	0.0084	0.0731	0.0072	0.0471	0.0073	0.0611
F	7.2	4	0.01	0.0058	0.0057	0.0651	0.0081	0.0373	0.0044	0.0641
F	7.2	5	0.0079	0.0062	0.009	0.0692	0.006	0.0418	0.0066	0.0708
F	9	1	0.009	0.0084	0.0034	0.065	0.0084	0.0495	0.0072	0.0621
F	9	2	0.0121	0.0067	0.0055	0.0726	0.0082	0.0484	0.0065	0.0595
F	9	3	0.0112	0.0056	0.006	0.0648	0.0071	0.034	0.0057	0.061
F	9	4	0.0132	0.0086	0.0059	0.0601	0.0062	0.0369	0.0058	0.0632
F	9	5	0.01	0.0076	0.008	0.0634	0.0078	0.0368	0.007	0.0683
F	10.8	1	0.0139	0.008	0.0073	0.071	0.0059	0.0453	0.0081	0.0619
F	10.8	2	0.0136	0.0083	0.0057	0.0694	0.0066	0.0458	0.0071	0.0603
F	10.8	3	0.0035	0.0181	0.0049	0.0819	0.0053	0.0529	0.0039	0.0714
F	10.8	4	0.0056	0.0194	0.0036	0.0752	0.0083	0.0472	0.0025	0.0622
F	10.8	5	0.2866	0.2173	20.5486	0.1514	0.1719	0.2391	4.1126	0.959

To explain why harmonic distortions were specifically calculated instead of just measuring leakage currents, Figure 3 was quoted to show the example of the recorded current signal for the selected case—that is, for a value of voltage equal to 7.2 kV and electrode configuration A. The distinctive courses from 1 to 5 represent the five gap distances considered. Figure 3a presents the original waveforms obtained during the measurements, while Figure 3b, in order to better visualize the similarities, shows the magnified fragments of the courses from Figure 3a.

As can be seen in Figure 3, no significant differences are observed between the collected leakage current signals. Hence, it is preferable to analyze the harmonic distortions, as this gives the possibility of performing meaningful comparisons between the cases considered. In detail, when the FFT analysis is performed (which is presented later in the paper), the effect of the applied voltage level, the electrode diameter, and the gaps between the electrodes on the partial discharge characteristics in the analyzed electrode system can be revealed significantly.

In general, it is important to emphasize herein that there is not a linearity between the electrode gap and grounded electrode diameter increase with the harmonic component change. In particular, specific changes in some harmonic distortions are remarkable. As is well-known, the capacitive reactance increases when the gap between electrodes is greater. However, within this experimental study, it is reported that the capacitive reactance, which was expected to increase with the increase in the electrode gap and the grounded electrode diameter, decreases at some voltage levels for some harmonic distortion levels, even if every parameter is kept the same.

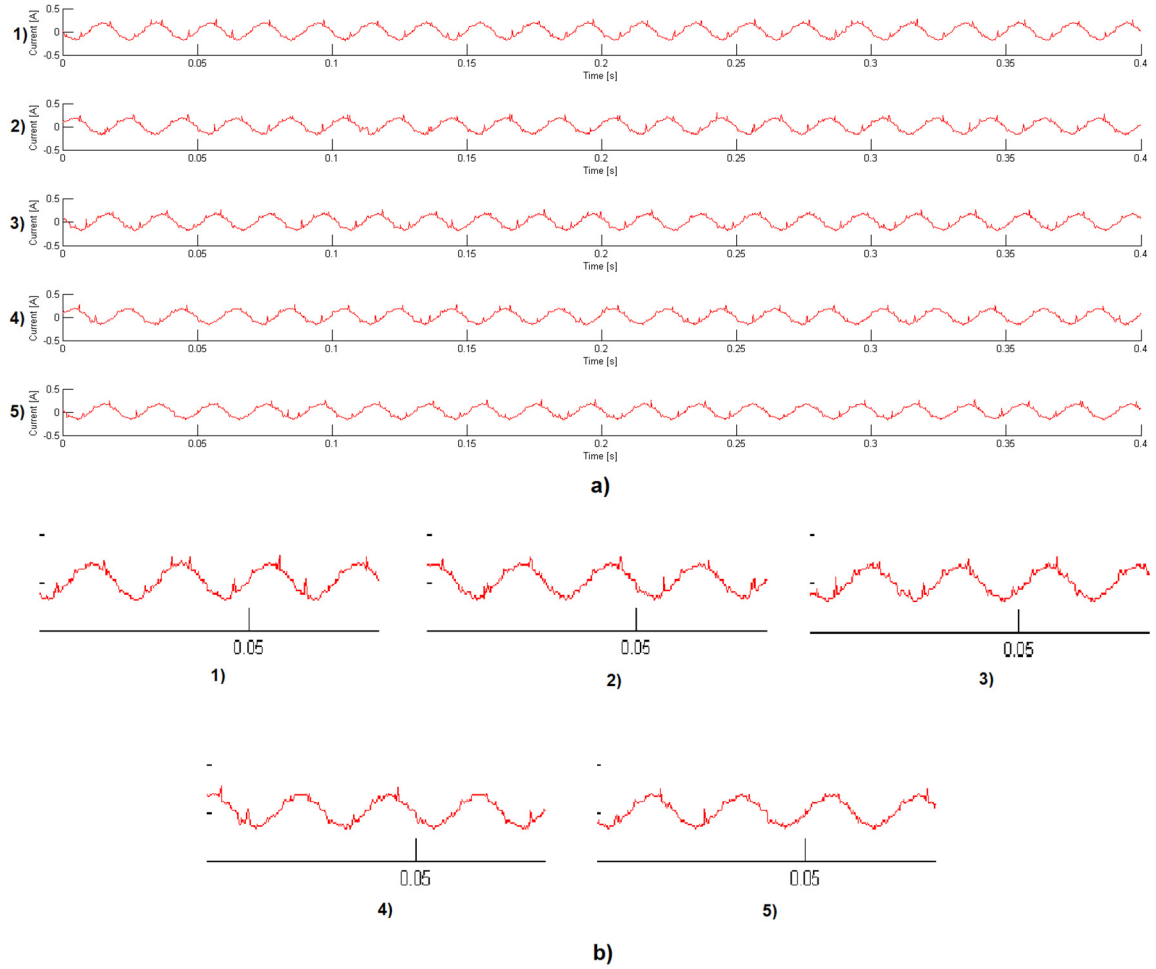

Figure 3. Current signal at electrode configuration A under a 7.2 kV voltage level and for the selected gap distances: (**a**) original waveforms; (**b**) magnified fragments of the waveforms; (**1**) 1, (**2**) 2, (**3**) 3, (**4**) 4, (**5**) 5 mm.

The current signals were more often distorted in the 1 and 2 mm gap distances, as seen in Figure 4 when comparing waveforms (1) and (2) with the other waveforms from this Figure. This is especially visible when observing the magnified fragment presented in Figure 4b. However, for a meaningful comparison of the PD behavior between the cases of the 1 and 2 mm gap distances, the proposed harmonic analysis method is needed. Additionally, for other electrode gaps, it is clearly seen in Figure 4 that it is so hard to analyze the PD behavior just by using the current signal. Hence, the proposed method of analyzing the FFT modified signals may give more information about the PD behavior in the analyzed electrode system immersed in oil.

The discharges seen in the oils cause the oil to locally warm up and eventually the oil to expand. This phenomenon is visible as the oil movement [11,20,24,34]. Such behavior of the oil was also observed during the studies performed herein, with a significant fluctuation in the oil during intensive discharges. In the following parts of the study, this movement made by the oil after the discharge appeared was considered in the analyses conducted. In some cases, the oil movement might eliminate the deteriorations in signals collected, especially when the distance increased to 5 mm. In such cases, no comparable harmonic distortion behavior was observed, and thus the harmonic components were evaluated as a possible source of information on PD activity, which is presented in the further part of the study.

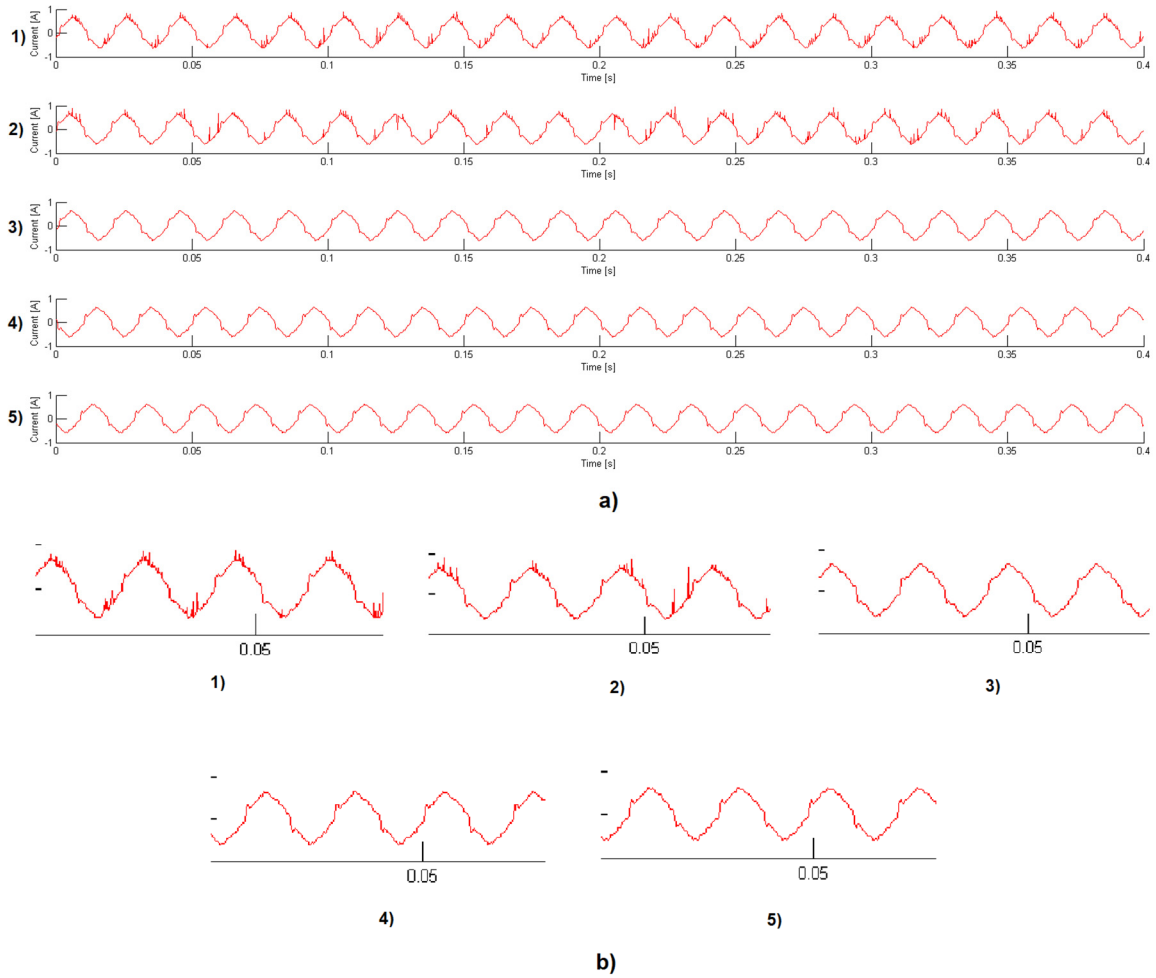

Figure 4. Current signal at electrode configuration E under a 10.8 kV voltage level and for the selected gap distances: (**a**) original waveforms; (**b**) magnified fragments of the waveforms; (**1**) 1, (**2**) 2, (**3**) 3, (**4**) 4, (**5**) 5 mm.

First, in Figure 5 in the form of a 3D chart, the data concerning configuration A are presented.

As can be seen from Figure 5 and simultaneously by analyzing the data from Table 2, it is first conspicuous that the value of the 5th harmonic for all electrode gaps and all voltage levels is the greatest. Due to the fact that the stimulated electrons at low voltage levels could not flow more easily into the grounded electrode, the potential capacitive effects around the electrodes at low voltage (5.4 kV) levels put forward the second harmonic (Penning effect) for this experiment. It is, however, well-known that the Penning effect is noted in the reactions between molecules and neutral atoms, and this is defined as chemi-ionization, especially occurring in gaseous insulators. Herein, this effect is referred to indicate that the 2nd harmonics arise from structures similar to chemical ionization [33,37,38].

It was observed also that the value of the 7th harmonic is greater at gaps of 4 mm between the electrodes, where harmonic distortion was observed intensely. The harmonic values at gaps of 1 mm between electrodes are expected to be higher due to the small electrode gap between the electrodes, which influences the value of electric field stress around the HV point. Since the closest gap between the electrodes is comparing the same value of testing voltage, a higher electrical field stress is created and more intense PDs occur with the higher generation of harmonics in the current signal. However, since the partial discharge is continuous at this gap, there are no sudden signal distortions. At the gaps of 3 and 4 mm, partial discharges from the leakage current signal are also noticed, and they are damped by the oil movement. Nevertheless, when partial discharge is initiated, since as the same time it can initiate harmonic distortions in the leakage current signal at a distance greater than the gap of

1 mm between electrodes, the harmonic distortion values here are high. In addition, it was observed that even the harmonic values were found to be higher.

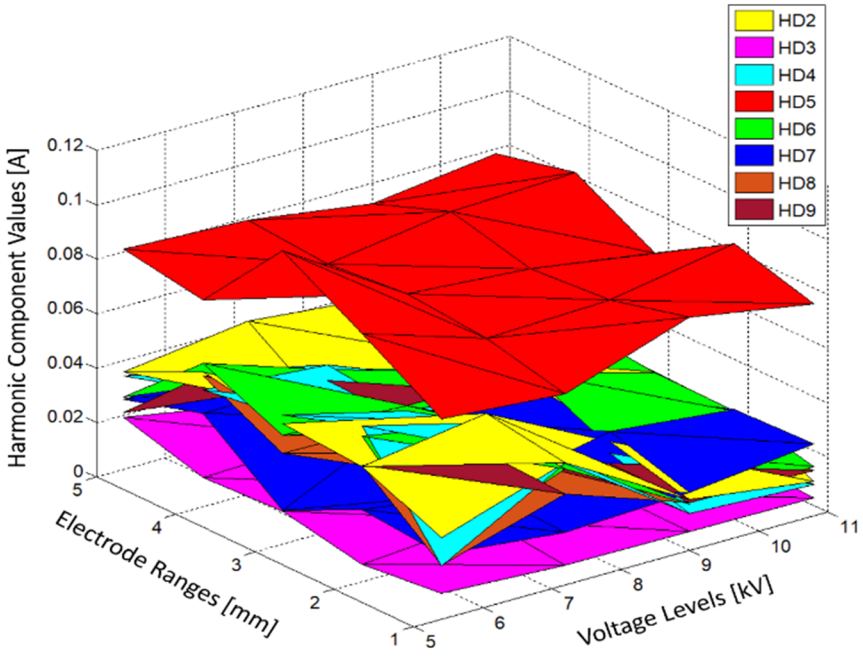

Figure 5. A 3D chart of the HD values for electrode configuration A and all voltage levels.

The results, in a similar way to those concerning the A configuration, are presented in Figure 6 for configuration B. When Table 2 and Figure 6 are examined at the 9 kV voltage level, it is seen that the harmonic values of the 2nd, 3rd, 4th, and 5th are higher at the gap of 2 mm compared to the harmonic values found for other electrode ranges. When the harmonic values are examined for all ranges, it is seen that the 5th harmonic values are 2–4 times higher than the other harmonic values.

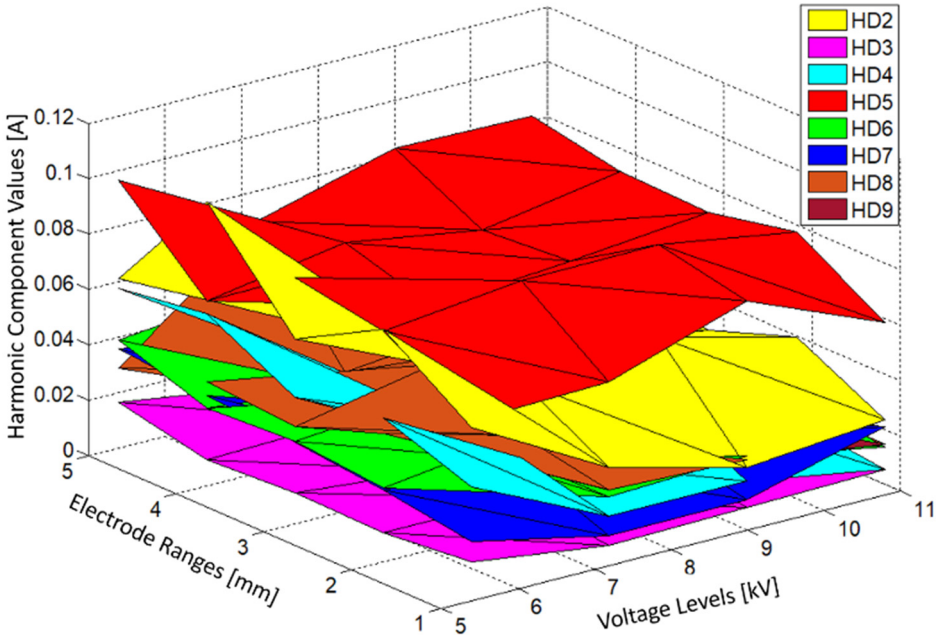

Figure 6. A 3D chart of the HD values for electrode configuration B and all voltage levels.

The steel (medical) needle has a lower electrical conductivity than the copper needle. Therefore, partial discharge started at a higher voltage level for the configurations based on this type of HV

electrode. This is because, in the case of gaseous or liquid insulation (mineral oil herein), PDs appear as a result of a local electric field stress increase, especially around the HV electrode. In such a case, the developing discharge needs energy for propagation, and this energy is ensured by fast electron movements (in the form of an electron avalanche) to the grounded electrode. In the initial phase of the PDs, they can continue their development through the electron movements. Additionally, when the number of electrons which are "knocked" from the HV electrode increase, the PD formation becomes faster. The conductivity of the electrode is thus important from the point of view of the number and accumulation of these movement electrons (the number of electrons in the avalanche). The more conductive a material is, more "knocked" electrons may take part in the discharge process [15,33]. Since the partial discharges at the 5.4 and 7.2 kV voltage levels have a low energy, no current signal is given in this section. The partial discharges began at 9 kV and have a high amplitude, especially at the gap of 2 mm. The current signal distortions at this range were seen at more points than for other ranges.

The results concerning configuration C are presented in Figure 7. In this electrode configuration, the diameter of the grounded electrode is smaller than that previously described. Thus, when a high voltage is applied, the distance it takes the free electrons to reach the sphere is shortened. The ionization path between the electrodes was shortened and partial discharge started earlier. In Figure 7, as the distance between the electrodes increases, the values of the harmonic components generally are less due to the oil movement as the ionization path increases.

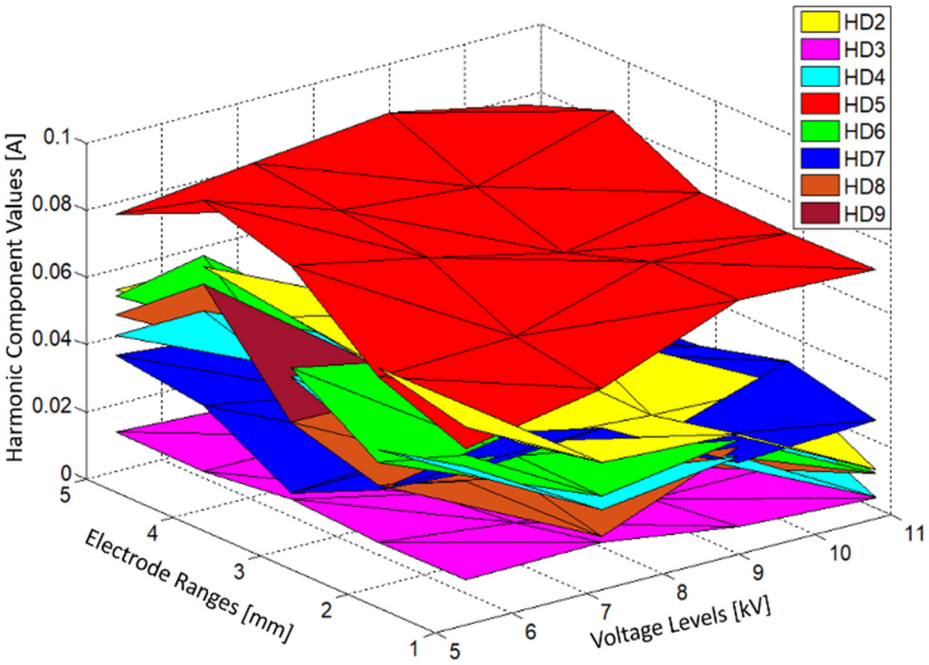

Figure 7. A 3D chart of the HD values for electrode configuration C and all voltage levels.

Analyzing jointly Table 2 and Figure 7 for all the electrode ranges, we can state that the 2nd and 5th harmonics predominantly have higher values than the others. In turn, the 6th harmonic value is higher than 2nd when the gap distance is 4 mm. When the 5th and 2nd harmonics are compared with each other, it is seen that value of the 2nd harmonic is higher at the 1 mm and 2 mm gaps. However, at the gaps of 3, 4, and 5 mm, the value of the 5th harmonic is higher. Even harmonics are known to occur when the oil movement decreases. Since the distance at which oil can move is increased at 3 mm and at higher distances, the 2nd harmonic value is less than the 5th harmonic.

Figure 8 shows the HD values for electrode configuration D when the high-voltage electrode is constituted of steel.

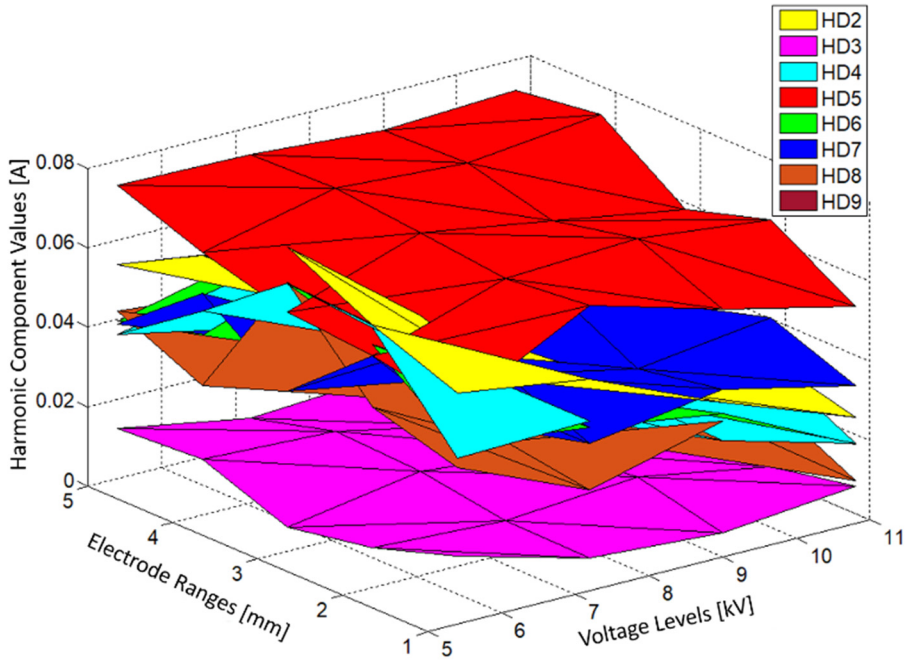

Figure 8. A 3D chart of the HD values for electrode configuration D and all voltage levels.

As can be seen in Figure 8, the harmonic distortion behavior in electrode configuration D is similar to the behavior in electrode configuration C. However, more ripples were formed at the 5.4 kV voltage level at the 2 and 3 mm distances. It can be obviously seen in Table 2 that the 2nd harmonic values at the gap of 1, 2, and 3 mm between electrodes are higher than the other harmonic values. The 5th harmonic value is the highest at the gaps of 4 and 5 mm. In addition, it is observed that the 3rd harmonic value decreases for the gaps 1, 2, and 3 mm and differs from the 5th harmonic value, but then increases again for the gaps of 4 and 5 mm.

For the E and F electrode configurations, the results are presented in Figures 9 and 10, respectively. The grounded electrode has, in these cases, a diameter of 2 cm. The harmonic component surfaces at electrode configuration E are shown in Figure 9.

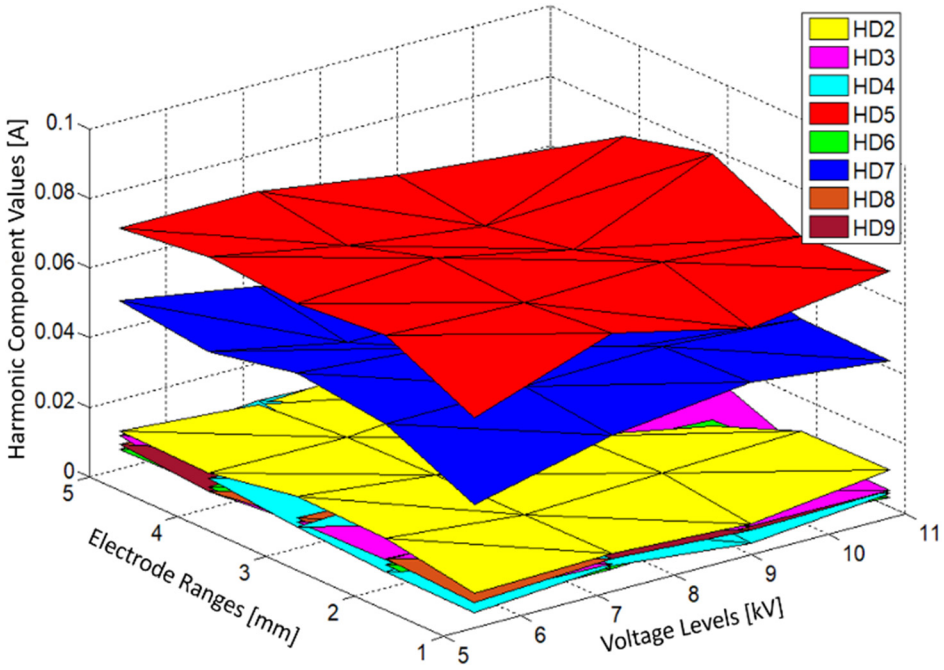

Figure 9. A 3D chart of the HD values for electrode configuration E and all voltage levels.

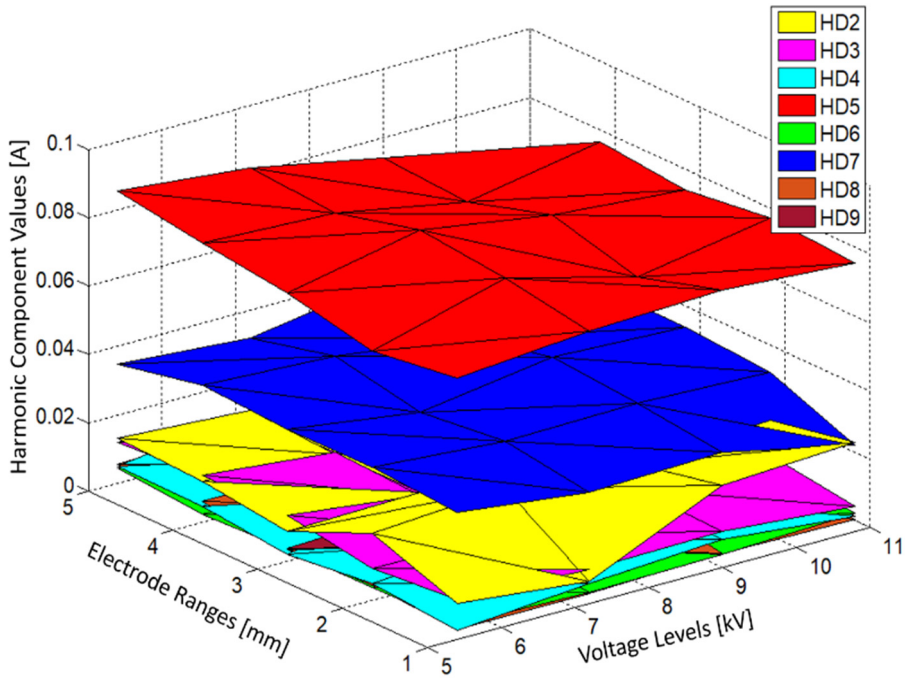

Figure 10. A 3D chart of the HD values for electrode configuration F and all voltage levels.

In this electrode configuration, characteristic points were formed during harmonic distortion at different electrode ranges at a voltage level of 9 kV. In Figure 9, the values of the 5th and 7th harmonics are significantly higher than the others and the 2nd harmonic is slightly higher. At the gap of 1 mm value the 5th harmonic is the highest, thereby at this distance the partial discharge and arc energy are reach the distorted value for the insulation strength. However, at the gap of 2 mm, the value of the 3rd harmonic was identified as higher than the counterparts in the other ranges.

The steel (medical) pointed-needle high-voltage electrode has a lower conductivity than the copper one used in the F-type electrode configuration. Therefore, in the case of configuration F the distortion in the signal is less than that of the E-type electrode configuration, which can be noticed from Figure 10. As shown also in Figure 10 and in Table 2, the 5th and 7th harmonic values are generally higher than the other harmonic values predominantly. At the gap of 2 mm, the value of the 5th harmonic component of the leakage current was the highest among all the harmonics. Conversely, at the gap of 1 mm the 4th harmonic value is lowest. The capacitive effect of the bubbles in the oil also caused the formation of even harmonics.

5. Conclusions

In the presented studies, a measurement method based on collecting the leakage currents through the grounded electrode under a non-uniform electric field was applied in order to assess the PD behavior in the designed electrode system immersed in mineral oil. To do this, the collected leakage currents were differentiated with FFT analysis and the harmonic distortion level was obtained.

From the results obtained, the following findings may be stated:

(1) By using the technique proposed in the paper, it was possible to measure the value of the leakage current corresponding with the partial discharges of corona type in oil at the different metal points, creating high-voltage electrode and different electric field distributions based on a non-invasive measurement technique.
(2) In all electrode configurations and gap distances, even harmonics components were measured.
(3) The amplitude of the 5th harmonic was noticed to be dominant in almost all cases, giving an unequivocal indication of which of the harmonic components can be used to identify the corona PDs in oil.

(4) The 2nd and 7th harmonics were also found to be clearly identified within the registered range of leakage current. They are characteristic in a slightly lower range for the configurations E and F, wherein the 7th harmonic has been identified with discharges for a small sphere creating the grounded electrode.

(5) It was observed that the calculated harmonic distortion values for all voltage levels increase when the sphere diameter decreases and the voltage level increases. This may be a result of the increase in the energy of the discharges formed.

(6) For the lowest voltage level, the harmonics (except the 5th and 9th harmonics) were measured to be higher in the case of the steel HV electrode, regardless of the gap distance between the electrodes. The reason for this may be attributed to the material (its conductivity) as the factor determining this finding.

(7) The studies allowed us to notice that the 7th harmonic is more visible when the E and F configurations were analyzed. This means that appearance of this harmonic may be accompanied by a higher level of electrical field uniformity.

(8) It has been observed that the 5th harmonics are the most recognized from others when the electric field uniformity reaches its maximum, as in the case of electrode configuration A.

(9) As the conductivity of the steel (medical) needle was less than that of the copper one, it was found that the harmonics were higher due to the conductivity disadvantage of the steel compared to the copper, and thus the electrode tip deformed faster.

(10) The measurements performed opened the way to continue studies of other electrode configurations, creating the systems generating surface-type PDs or PDs in internal cavities. Such studies are being planned by the authors to be performed in the near future. In the studies planned, also other dielectric liquids such as synthetic and natural esters will be considered as possible sources of changes in the registered quantities. An important part of the future studies will be also the verification of the correlation between the PDs' behavior and harmonics using the methods based on indexes of similarity, such as Pendry, van Hove, Integrated against Error Log Frequency (IELF), or Frequency Selective Validation (FSV) [39].

Author Contributions: Conceptualization, A.E.Y.; methodology, A.E.Y.; software, A.A.; validation, A.E.Y. and P.R.; formal analysis, F.A. and P.R.; investigation, F.A.; resources, A.A.; data curation, A.A.; writing—original draft preparation, A.A., F.A., and P.R.; writing—review and editing, F.A. and P.R.; visualization, F.A.; supervision, A.E.Y.; project administration, A.E.Y.; funding acquisition, A.A. All authors have read and agreed to the published version of the manuscript.

Funding: This work was supported by the Istanbul University-Cerrahpaşa Scientific Research Projects Executive Secretariat with the Project number of 33689.

Conflicts of Interest: The authors declare no conflict of interest.

References

1. Li, S.; Yu, S.; Feng, Y. Progress in and prospects for electrical insulating materials. *High Volt.* **2016**, *1*, 122–129. [CrossRef]
2. Fofana, I. 50 Years in the development of insulating liquids. *IEEE Electr. Insul. Mag.* **2013**, *29*, 13–25. [CrossRef]
3. Lu, W.; Liu, Q. Effect of cellulose particles on streamer initiation and propagation in dielectric liquids. In Proceedings of the IEEE 11th International Conference on the Properties and Applications of Dielectric Materials (ICPADM), Sydney, Australia, 19–22 July 2015; pp. 939–942. [CrossRef]
4. Zhang, J.; Li, J.; Huang, D.; Zhang, X.; Liang, S.; Li, X. Influence of Nonmetallic Particles on the Breakdown Strength of Vegetable Insulating Oil. In Proceedings of the 2015 IEEE Conference on Electrical Insulation and Dielectric Phenomena (CEIDP), Ann Arbor, MI, USA, 18–21 October 2015; pp. 609–612. [CrossRef]
5. Tao, Z.; Yunpeng, L.; Fangcheng, L.; Ruihong, D. Study on dynamics of the bubble in transformer oil under non-uniform electric field. *IET Sci. Meas. Technol.* **2016**, *10*, 498–504. [CrossRef]

6. Berg, G.; Lundgaard, L.E.; Becidan, M.; Sigrnond, R.S. Instability of electrically stressed water droplets in oil. In Proceedings of the IEEE 14th International Conference on Dielectric Liquids (ICDL), Graz, Austria, 12–12 July 2002; pp. 220–224. [CrossRef]
7. Yilmaz, H.; Guler, S. The effect of electrode shape, gap and moisture on dielectric breakdown of transformer oil. In Proceedings of the 12th International Conference on Conduction and Breakdown in Dielectric Liquids (ICDL), Roma, Italy, 15–19 July 1996; pp. 354–357. [CrossRef]
8. Uzunoğlu, C.P. A Comparative study of empirical and variational mode decomposition on high voltage discharges. *Electrica* **2018**, *18*, 72–77. [CrossRef]
9. Piotrowski, T.; Rozga, P.; Kozak, R. Analysis of excessive hydrogen generation in transformers in service. *IEEE Trans. Dielectr. Electr. Insul.* **2015**, *22*, 3600–3607. [CrossRef]
10. Dombek, G.; Nadolny, Z. Liquid kind, temperature, moisture, and ageing as an operating parameters conditioning reliability of transformer cooling system. *Maint. Reliab.* **2016**, *18*, 413–417. [CrossRef]
11. Rozga, P.; Stanek, M.; Rapp, K. Lightning properties of selected insulating synthetic esters and mineral oil in point-to-sphere electrode system. *IEEE Trans. Dielectr. Electr. Insul.* **2018**, *25*, 1699–1705. [CrossRef]
12. Khaled, U.; Beroual, A. AC dielectric strength of mineral oil-based Fe_3O_4 and Al_2O_3 nanofluids. *Energies* **2018**, *11*, 3505. [CrossRef]
13. *High-Voltage Test Techniques—Partial Discharge Measurements*; IEC Standard 60270; International Electrotechnical Commission: Geneva, Switzerland, 2000.
14. Ersoy, A. Investıgatıng Boron Contrıbutıons and Electrıcal Properties of Polymerıc Insulators Used in Electrıcal Insulatıon Systems. Ph.D. Dissertation, Institute of Science and Technology, Istanbul University, Istanbul, Turkey, 2007.
15. Bartnikas, R. Partial discharges. Their mechanism, detection and measurement. *IEEE Trans. Dielectr. Electr. Insul.* **2002**, *9*, 763–808. [CrossRef]
16. Kunicki, M.; Cichon, A.; Nagi, L. Statistics based method for partial discharge identification in oil paper insulation systems. *Electr. Power Syst. Res.* **2018**, *163*, 559–571. [CrossRef]
17. Zhao, J.; An, Z.; Lv, B.; Wu, Z.; Zhang, Q. Characteristics of the partial discharge in the development of conductive particle-initiated flashover of a GIS Insulator. *Energies* **2020**, *13*, 2481. [CrossRef]
18. Abu-Siada, A. Improved consistent interpretation approach of fault type within power transformers using dissolved gas analysis and gene expression programming. *Energies* **2019**, *12*, 730. [CrossRef]
19. Sikorski, W. Active dielectric window: A new concept of combined acoustic emission and electromagnetic partial discharge detector for power transformers. *Energies* **2019**, *12*, 115. [CrossRef]
20. Kunicki, M.; Cichon, A.; Borucki, S. Measurements on partial discharge in on-site operating power transformer: A case study. *IET Gener. Transm. Distrib.* **2018**, *12*, 2487–2495. [CrossRef]
21. Walczak, K.; Sikorski, W.; Gil, W. Multi-module system for partial discharge monitoring using AE, HF and UHF methods. *Prz. Elektrotech.* **2016**, *92*, 5–9. [CrossRef]
22. Liang, R.; Wu, S.; Chi, P.; Peng, N.; Li, Y. Optimal placement of UHF sensors for accurate localization of partial discharge source in GIS. *Energies* **2019**, *12*, 1173. [CrossRef]
23. Florkowski, M.; Krzesniak, D.; Kuniewski, M.; Zydron, P. Partial Discharge Imaging Correlated with Phase-Resolved Patterns in Non-Uniform Electric Fields with Various Dielectric Barrier Materials. *Energies* **2020**, *13*, 2676. [CrossRef]
24. Koziol, M. Energy distribution of optical radiation emitted by electrical discharges in insulating liquids. *Energies* **2020**, *13*, 2172. [CrossRef]
25. *Partial Discharges in Transformer Insulation*; CIGRE Task Force 15.01.04; International Council on Large Electric Systems (CIGRE): Paris, France, 2000.
26. Chen, W.; Chen, X.; Peng, S.; Li, J. Canonical correlation between partial discharges and gas formation in transformer oil paper insulation. *Energies* **2012**, *5*, 1081–1097. [CrossRef]
27. Kreuger, F.H.; Gulski, E.; Krivda, A. Classification of partial discharges. *IEEE Trans. Electr. Insul.* **1993**, *28*, 917–931. [CrossRef]
28. Gulski, E.; Kreuger, F.H. Computer-aided recognition of discharge sources. *IEEE Trans. Electr. Insul.* **1992**, *27*, 82–92. [CrossRef]
29. Cavallini, A.; Contin, A.; Montanari, G.C.; Puletti, F. Advanced PD inference in on-field measurements. I. Noise rejection. *IEEE Trans. Dielectr. Electr. Insul.* **2003**, *10*, 216–224. [CrossRef]

30. Cavallini, A.; Conti, M.; Contin, A.; Montanari, G.C. Advanced PD inference in on-field measurements. II. Identification of defects in solid insulation systems. *IEEE Trans. Dielectr. Electr. Insul.* **2003**, *10*, 528–538. [CrossRef]
31. Contin, A.; Pastore, S. Classification and separation of partial discharge signals by means of their auto-correlation function evaluation. *IEEE Trans. Dielectr. Electr. Insul.* **2009**, *16*, 1609–1622. [CrossRef]
32. Alvarez, F.; Ortego, J.; Garnacho, F.; Sanchez-Uran, M.A. A clustering technique for partial discharge and noise sources identification in power cables by means of waveform parameters. *IEEE Trans. Dielectr. Electr. Insul.* **2016**, *23*, 469–481. [CrossRef]
33. Kufel, E.; Zaengl, W.S.; Kufel, J. *High Voltage Engineering—Fundamentals*, 2nd ed.; Elsevier: Oxford, UK, 2000.
34. *Fluids for Electrotechnical Applications—Unused Mineral Insulating Oils for Transformers and Switchgear*; IEC Standard 60296; International Electrotechnical Commission: Geneva, Switzerland, 2003.
35. Patrissi, S.; Pompili, M.; Yamashita, H.; Forster, E.O. A study of the effect of electrical breakdown in dielectric liquids on the needle point structure. In Proceedings of the IEEE 11th International Conference on Conduction and Breakdown in Dielectric Liquids, Baden-Dättwil, Switzerland, 19–23 July 1993; pp. 376–382. [CrossRef]
36. Lesaint, O. Prebreakdown phenomena in liquids: Propagation modes and basic physical properties. *J. Phys. D Appl. Phys.* **2016**, *49*, 14401–14422. [CrossRef]
37. Falcinelli, S.; Candori, P.; Bettoni, M.; Pirani, F.; Vecchiocattivi, F. Penning ionization electron spectroscopy of hydrogen sulfide by metastable helium and neon atoms. *J. Phys. Chem. A.* **2014**, *118*, 6501–6506. [CrossRef] [PubMed]
38. Korenev, S. The internal Penning Ion Source of negative hydrogen ions for isochronous cyclotrons. In Proceedings of the IEEE Pulsed Power Conference (PPC), Austin, TX, USA, 31 May–4 June 2015; pp. 1–6. [CrossRef]
39. Bongiorno, J.; Mariscotti, A. Evaluation of performances of indexes used for validation of simulation models based on real cases. *Int. J. Math. Models Methods Appl. Sci.* **2015**, *9*, 29–43.